Separation and Purification Technology 316 (2023) 123818

Contents lists available at ScienceDirect

Separation and Purification Technology

journal homepage: www.elsevier.com/locate/seppur

A chemically tailored capacitive deionization system for the enhanced removal of cesium from process water

Jiming Lu [a,b], Qiurong Long [a], Yi Liu [a], Binda Lu [a], Jiaxin Hu [b], Fan Yang [c], Feng Jiang [a], Timothy N. Hunter [b], Zhouguang Lu [a], David Harbottle [b,*], Zhenghe Xu [a,*]

[a] Shenzhen Key Laboratory of Interfacial Science and Engineering of Materials, Department of Materials Science & Engineering, Southern University of Science and Technology, Guangdong, PR China
[b] School of Chemical and Process Engineering, University of Leeds, Leeds LS2 9JT, UK
[c] College of New Materials and New Energies, Shenzhen Technology University, Shenzhen 518118, PR China

ARTICLE INFO

Keywords:
Capacitive deionization
Cesium
Spent fuel liquor
MXene
EDTA
Enrichment

ABSTRACT

A capacitive deionization (CDI) electrode comprising ethylenediamine triacetic acid (EDTA) and 2D MXene (EDTA-MXene) is fabricated to separate Cs^+ from strongly acidic process water. The method provides new direction for an advanced aqueous recycle process to separate fission products from spent fuel liquor. Grafting EDTA on MXene has no detrimental effect on its structure but does diversify the modes of ion interaction and increase the number of binding sites. The composite CDI electrode has a Cs^+ adsorption capacity of 2.07 mmol g^{-1} at 1.2 V with 97.3% removal efficiency within 15 min. Step-wise adsorption and desorption cycling of the electrode highlights the chemisorption effect of EDTA which immobilizes the ions as the applied voltage is lowered, although almost all ions can be stripped by reversing the voltage to −1.4 V and without the need for chemical treatment. The EDTA-MXene electrode demonstrates outstanding cyclic performance with a capacity retention of >80% after 320 cycles. Furthermore, the electrode maintains its performance in strongly acidic solution, removing 0.66 mmol g^{-1} Cs^+ at 1.2 V, as well as being stable after immersing in 3 mol L^{-1} HNO_3 for 7 days. Through continuous cycling it is possible to enrich the Cs^+ into a highly concentrated solution for element recovery or safe disposal. The EDTA-MXene material is robust and maintains good performance in harsh chemical environments, levering its multiple binding sites to successfully isolate Cs^+ from strongly acidic solutions and in the presence of competing ions, Sr^{2+} and Ce(IV).

1. Introduction

The demand for electricity is rapidly increasing and nuclear power is a viable option to meet demand and not compromise the net zero agenda. With expansion of the nuclear fleet, the technology used in the closed-cycle process must be reevaluated so that other desirable elements can be efficiently recovered to provide sustainability to the industry.

Closed-cycle systems such as the Plutonium Uranium Reduction Extraction (PUREX) process or variations thereof, are currently used to separate U and Pu from fission products [1]. However, redesigning the flowsheet to expand the range of species recovered is desired in future operations of aqueous recycle. New approaches to separation must increase recovery of valuable elements, lessen or eliminate the use of toxic extractants, lower the cost of extraction, and reduce the waste volume sent to a geological disposal facility.

Capacitive deionization (CDI) has shown great potential to decontaminate complex effluents. Similar to a capacitor, CDI treats effluents by immobilizing ions within the electrical double layer of the electrode surface [2–4]. Its use has already been demonstrated to recover U(VI) from simulated process water, but the recovery of fission products by CDI is less studied [5–8]. Relatively simple electrode materials such as activated carbon fibres [9], as well as more elaborate materials, such as a tungsten trioxide and carbon (WO_3/C) composite [10], and porous chitosan and biocarbon composite [11], have shown good recovery of U (VI), with the best reported extraction of 449 mg g^{-1} at 1.2 V, although electrode regeneration (consecutive cycles of ion adsorption and desorption) has shown limited performance with capacity dropping to 90% after 5 cycles [10].

The removal of fission products by CDI has rarely been explored

* Corresponding authors.
E-mail address: D.Harbottle@leeds.ac.uk (D. Harbottle).

https://doi.org/10.1016/j.seppur.2023.123818
Received 14 November 2022; Received in revised form 26 March 2023; Accepted 6 April 2023
Available online 8 April 2023

using MXene as the electrode template [12]. However, its use as an adsorbent is extensively studied because of its two-dimensional layered structure, rich elemental composition, and surface chemistry. Khan et al. [13] used $Ti_3C_2T_x$ to adsorb Cs^+ from simulated wastewater, exploiting the materials -OH, -O and -F groups to act as binding sites for Cs^+, although its adsorption capacity remained low at 25 mg g^{-1}. Jun et al. [14] could increase capacity to 148 mg g^{-1} by finding the optimal test conditions (Cs^+ concentration, pH, temperature and adsorption time), however, regeneration of the pristine MXene was poor and removal efficiency dropped below 70% after 4 cycles. Shahzad et al. [15] prepared MXene aerogel spheres coated with Prussian blue to give selective binding to Cs^+. The composite had a Cs^+ adsorption capacity of 316 mg g^{-1}, but when dispersed in HNO_3 solutions, the sorbent was found to be ineffective and the removal efficiency dropped below 20%. Loss of performance in strongly acidic solutions is commonly seen because of issues relating to material stability and/or limited ion exchange/adsorption due to the effects of protonation [16–18]. As such, few studies have tested the performance of adsorbents under process relevant conditions. Given its excellent electrical conductivity, good mechanical stability [19] and versatile interaction pathways for adsorbing radionuclides [20], MXene has many desirable properties for it to perform under harsh conditions.

Although efforts have been made to modify the MXene surface to recover radionuclides, as highlighted, more effective functionalization of MXene is needed to overcome current limitations and make the approach more practical for industry. In the current study, an EDTA-MXene composite (Fig. 1) was prepared so that the grafted-EDTA provides specific binding sites to firmly immobilize Cs^+. Furthermore, when combined with CDI, the adsorption capacity of the material can be modulated by the applied voltage, and so the material can be regenerated for reuse. The method is a technological step-forward as it allows for the stripping of radionuclides by the simple reversal of the applied voltage, providing a route for extraction and enrichment without using toxic extractants.

2. Materials and methods

2.1. Synthesis of MXene

Ti_3AlC_2 (99%, 400 mesh, Ningbo Jinlei Biotech Co.) was etched using aqueous HF solution (48%, Aladdin) at a solid-to-liquid mass ratio of 1:10 (1 g Ti_3AlC_2 and 8.67 mL HF). The suspension was magnetically stirred for 4 h at 60 °C, before recovering the particles by centrifuging at 10,000 rpm for 15 min. The sediment was repeatability washed using deionized water until the filtrate pH was 7 and dried in a vacuum oven at −1 bar for 12 h at 60 °C. Generally, the dilute HF in the wastewater of this experiment can be detoxified by precipitation with addition of $CaCl_2$ to form CaF_2 precipitates while the concentrated HF could be reused. The resultant CaF_2 is highly insoluble in water and can be collected for safe disposal. It should be noted that with great care, the use of HF could be well controlled and recycled as encountered in semiconductor and microelectronics industries [21]. While the HF method is commonly used to prepare MXene, it is worth noting that HF-free routes such as electrochemical etching potentially offer a green route for their preparation. The method etches Al from porous Ti_2AlC using HCl solution, but the time needed for etching is several days [22], substantially longer than the current method. While greener routes are being developed, they do lack scalability, unlike the wet etching process as described here [23], and so there remains a compromise which is still to be solved.

2.2. Preparation of EDTA-MXene

The EDTA-MXene was prepared by a facile liquid phase reaction following a previously reported method [24], see Fig. 1. The method allows the hydroxyl groups of EDTA-silane to react with the hydroxyl groups on the surface of MXene that are generated during the etching process. Firstly, 120 mg of MXene was dispersed in 300 mL ethanol and ultrasonicated for 2 h. The dispersion was then mixed with 50 mL EDTA-silane (MW 462.4, 2.0% v/v, J&K Scientific) under gentle magnetic stirring for 12 h at 65℃. The particles were recovered following the same method used to prepare the MXene particles.

2.3. Electron microscopy

A high-resolution TEM (FEI Titan Themis Cubed 300 microscope, Thermo Fisher Scientific) operated at 300 kV was used to image the layered structure of the prepared particles. The particles were dispersed in ethanol at 1000 ppm and ultrasonicated for 5 min before depositing one drop of the suspension onto a copper grid of an amorphous carbon film (Beijing Zhongjingkeyi Technology Co., Ltd.) and dried under an infrared lamp.

A TM3030Plus SEM (Hitachi) with energy dispersive X-ray spectroscopy (EDX, Oxford Instruments, X-stream-2) was used to determine the morphology and elemental composition of the particles. The acceleration voltage was set at 10 kV with a working distance of 8 mm. Samples were prepared following the previously described method and deposited onto a single-crystal silicon wafer.

2.4. Fourier transform infrared spectroscopy

FTIR was used to determine the surface chemistry of MXene and EDTA-MXene. The samples were mixed with KBr by strong vibration and the mixture pressed into a 10 μm thick pellet. A Nicolet iS10 FT-IR spectrometer equipped with a deuterated triglycine sulphate (DTGS)

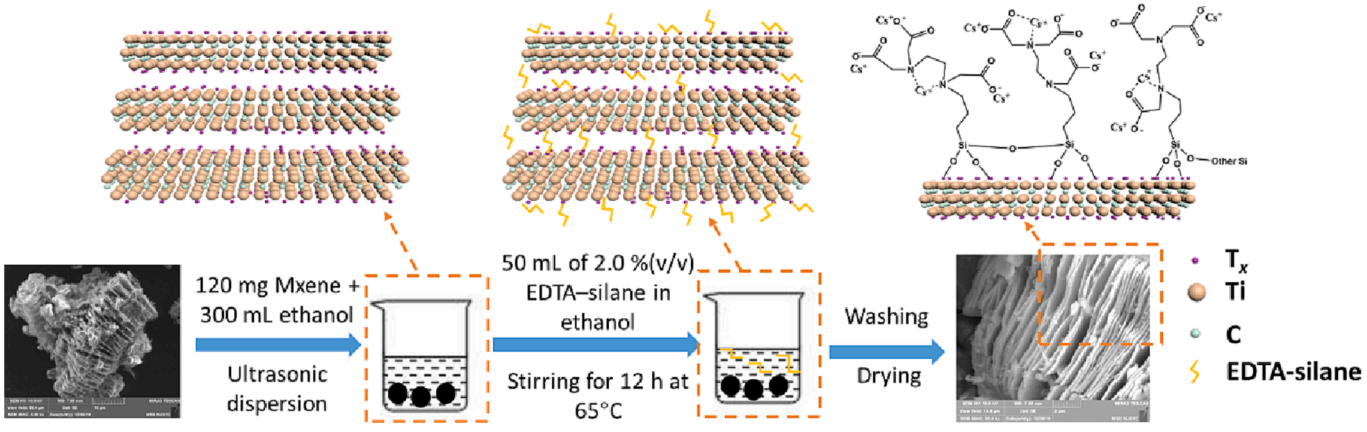

Fig. 1. Flow diagram highlighting the key steps to convert MXene to EDTA-MXene. T_x: terminal functional groups such as OH^- and F^-.

KBr detector was used.

2.5. X-ray photoelectron spectroscopy

The surface chemistry of MXene and EDTA-MXene was determined using XPS (VG Multilab 2000) with a monochromated Al Kα X-ray source of 1486.6 eV (Thermo Fisher, Escalab 250Xi, USA). Samples were placed in the XPS chamber that was maintained under 10^{-7} Pa of vacuum. Charge build-up on the samples was compensated by an electron/ion gun. All spectra were calibrated against the C 1 s peak (285 eV) and deconvoluted using the Avantage software of Powell fitting algorithm with Gauss-Lorentz mix product and 0.0001 convergence value.

2.6. Thermogravimetric analysis

The amount of EDTA loaded onto the MXene substrate was approximated from TGA. 10 mg samples were placed into a STA449F3 TGA (NETZSCH, Germany) and heated from 25 to 1000°C at a heating rate of 10 K/min with a gentle purge of argon.

2.7. Electrode preparation and metal ion adsorption

The CDI electrodes were prepared by milling the active material (MXene or EDTA-MXene), Super P® (Kejing Ltd.) and polyvinylidene fluoride (PVDF, Sigma Aldrich) at a mass ratio of 8:1:1 in N-methylpyrrolidone (NMP) using an agate mortar for 1 h. The slurry was then coated onto a 10 μm thick graphite paper (Jinlong International Carbon Group) using a film applicator machine (MSK-AFA-ES200, Kejing Ltd.) with a gap spacing of 100 μm and a coater speed of 3 mm/s. The film was dried in a vacuum oven at 80 °C for 12 h and then cut to size (80 × 80 mm) so that each electrode contained 200 mg of the active material.

The recovery of Cs^+ by MXene and EDTA-MXene was studied using a continuous CDI system which included a custom-built CDI cell, power source (RXN-605D, Zhaoxin), peristaltic pump (BT100-2J, Lange), conductivity meter (Type 308A, Leici Company) and 500 mL feed and discharge beakers. For each CDI test, 200 mL of contaminated water was cycled through the CDI cell at 20 mL/min while applying a direct voltage of 0 V (open circuit) or 1.2 V (closed circuit). A 1-mm thick silicon rubber seal was used to separate the CDI electrodes: working electrode, MXene or EDTA-MXene; counter electrode, graphite paper. The Cs^+ concentration was varied from 0.2 to 2 mmol L^{-1} and the solution pH maintained at 5.0 ± 0.1. The residual ion concentration in solution after adsorption was measured by atomic absorption spectroscopy (AAS, 200 Series AA, Agilent Technologies). The adsorption capacities (Q_e) of the electrodes were calculated by [25]:

$$Q_e = \frac{(C_0 - C_e)V}{m} \tag{1}$$

where C_0 and C_e (mmol L^{-1}) represent the initial and equilibrium ion concentrations, respectively, V (L) the solution volume, and m (g) the mass of active material (not including the mass of binder and conductive agent) in the electrode.

The isotherm data was fitted using the Langmuir adsorption model (Eq. (2)) which implies a monolayer adsorption of Cs^+ on the electrode surface:

$$Q_e = \frac{Q_0 K_L C_e}{1 + K_L C_e} \tag{2}$$

The linearized form of Eq. (2) is given by Eq. (3):

$$\frac{1}{Q_e} = \frac{1}{Q_0} + \frac{1}{Q_0 K_L C_e} \tag{3}$$

where Q_e is the equilibrium adsorption capacity (mmol g^{-1}) at the equilibrium concentration, C_e (mmol L^{-1}), Q_o is the theoretical maximum adsorption capacity (mmol g^{-1}) of the electrode, and K_L (L mmol^{-1}) is the Langmuir adsorption constant which describes the affinity between the ions and binding sites.

2.8. Adsorption kinetics

The electrodes were evaluated using the CDI setup operating with an applied voltage of 0 V or 1.2 V. Test solutions of 200 mL were prepared at C_0 of 0.5 mmol L^{-1} Cs^+ and recirculated through the CDI cell at a flow rate of 20 mL/min. The residual concentration (C_t – time dependent concentration) was measured at 5, 15, 30, 45, 60, 90 and 120 min. The adsorption kinetic data was fitted to the pseudo-second order rate equation (PSORE) [26]:

$$\frac{t}{Qt} = \frac{1}{k_2 Q_e^2} + \frac{t}{Q_e} \tag{4}$$

where Q_t (mmol g^{-1}) and Q_e (mmol g^{-1}) refer to the quantity of adsorbed ions at times t and at equilibrium, and k_2 represents the adsorption rate constant.

2.9. Competitive adsorption

The effect of HNO_3 on the Cs^+ adsorption capacity of the electrodes was evaluated using the CDI cell operating at 1.2 V. Test solutions of 100 mL were prepared to 0.75 mmol L^{-1} Cs^+ with different concentrations of HNO_3 from 0 to 3 mol L^{-1}. The test solutions were recirculated through the CDI cell at a flow rate of 0.8 mL/min for 125 min.

2.10. Electrochemical performance

The electrochemical performances of the MXene and MXene-EDTA electrodes were measured using a three-electrode setup which included a working electrode (MXene, EDTA-MXene), a Pt mesh counter electrode and an Ag/AgCl reference electrode. A CHI 604E electrochemical workstation (CH Instruments, Inc, China) was used, and the test solution was either 0.5 mmol L^{-1} CsCl or 0.5 mmol L^{-1} CsCl with 2 mol L^{-1} HNO_3. For cyclic voltammetry (CV) the voltage was varied between 0 and 1.2 V at a scan rate of 20 mV s^{-1}. Electrical impedance spectroscopy (EIS) was conducted in the frequency range of 0.01 Hz to 100 kHz with an alternating current (AC) amplitude of 5 mV. Galvanostatic charge–discharge (GCD) measurements were performed between 0 and 1 V at a current density of 0.5 A g^{-1}.

Using the CV data, the specific capacitance (C, F g^{-1}) can be determined by [27]:

$$C = \frac{\int IdV}{2mv\Delta V} \tag{5}$$

where I is the current density (A g^{-1}), m is the mass of active material in the working electrode (g), v is the scan rate (V s^{-1}), and ΔV is the potential window (V).

2.11. Electrode durability

The electrode loading capacity was measured by varying the applied voltage between −1.4 to 1.6 V. Although the voltage was occasionally higher than the critical voltage for water electrolysis (1.23 V in pure water), no visible signs of water electrolysis were observed and it is known that adding salt to pure water increases the voltage limit [28], hence water electrolysis was not a concern in the current study. Using test solutions of 0.5 mmol L^{-1} Cs^+, 200 mL of the test fluid was recirculated through the CDI cell at 20 mL/min for 30 min. An asymmetric CDI configuration was used where the anode was graphite paper (adsorption capacity for Cs^+ was 0.045 mmol g^{-1}) and the cathode either EDTA-MXene or MXene. The applied voltage was adjusted between 0 V and 1.6 V to study the effect of voltage on adsorption, and for desorption, the CDI electrode was first operated with a voltage of 1.6 V

for 30 min, before lowering the voltage to desired level and holding for 30 min. The test solution was then sampled and the ion concentration measured by AAS.

The regeneration of the as-prepared electrodes was studied using the asymmetric CDI cell configuration. The applied voltage was alternated between 1.2 V (adsorption) and −1.4 V (desorption). Test solutions of 200 mL and 0.5 mmol L^{-1} Cs^+ were recirculated through the CDI cell at 20 mL/min. For each adsorption and desorption step, the applied voltage was kept constant for 30 min, i.e. 1 h per cycle. The total testing time was 320 h and so 320 cycles. After each 10 cycles the test solution was sampled to determine the amount of Cs^+ adsorbed by the electrode (q_x). The capacity retention is given by q_x/q_{1st}, where q_x is the adsorption capacity at x cycles, and q_{1st} is the adsorption capacity at the first cycle. During the first 3 cycles, a conductivity meter was used to monitor the conductivity changes of test fluids.

The ability to enrich waste solutions was assessed using the setup shown in Figure S1 of the Supporting Information. The test solution of 500 mL of 0.5 mmol L^{-1} Cs^+ was pumped at 50 mL/min for 30 min and recirculated through the CDI cell that was operated with an applied voltage of 1.2 V. The flow was then switched to the enrichment tank so that the Cs^+ could be desorbed into 50 mL of deionized water, with the CDI voltage reversed to −1.4 V for 30 min. This process of switching between two flow lines was repeated 10 times. While the enriched fluid was not replaced, a fresh feed solution was used each time so as not to deplete the Cs^+ concentration in the feed. To determine the limit of enrichment, a second test was undertaken using 50 mL of 75 mmol L^{-1} Cs^+ (~10,000 ppm) as the solution in the enrichment tank. The same test protocol was repeated, but the starting concentration in the enrichment tank was significantly higher.

3. Results and discussion

The morphologies of MXene and EDTA-MXene were confirmed by SEM and TEM imaging. Both materials are composed of thin Ti_3C_2 layers of approximately 0.85 nm thickness and form an accordion-like morphology (Fig. 2a and d), confirming the successful etching of the MAX phase [29]. An SEM image of the MAX phase is provided in Figure S2 for comparison. BET surface area analysis revealed the specific surfaces areas of MXene and EDTA-MXene to be 20.2 and 26.5 m^2 g^{-1}, respectively. The low surface area confirms the low porosity of both samples after the HF etching process. High-resolution TEM images (Fig. 2b and e) and the corresponding selected area electron diffraction (SAED) patterns (Fig. 2c and f) of MXene and EDTA-MXene confirm both materials retain the hexagonal structure of the MAX phase [29,30]. Measurement of the lattice leads to the labelled Ti_3C_2 crystal, with corresponding lattice planes of (0 1 0 0) and (1 0 $\bar{1}$ 0)[29,30].

XRD further confirmed the crystal structure of MXene and EDTA-MXene (Fig. 3a). Compared with the diffraction peaks of MAX, most of the non-basal plane peaks (strongest peak at 39°) disappeared after etching with HF. Furthermore, the peaks at 9.8° and 18° shifted to lower 2θ values of 8.2° and 16.7°, confirming the interlayer expansion of MXene compared to MAX [29]. These findings validate the successful preparation of MXene. It is interesting to note a negligible difference between MXene and EDTA-MXene, implying that the grafting of EDTA has no discernable influence on the crystal structure of MXene. From TGA, the amount of EDTA grafted on MXene surface was 0.403 mmol g^{-1}, see Fig. S3a of the Supporting Information which compares the thermograms of MXene and EDTA-MXene. Furthermore, EDS analysis of EDTA-MXene (Fig. S2) confirmed a homogeneous distribution of EDTA on the MXene surface.

The surface chemistry was evaluated by FTIR. As shown in Fig. 3b, the spectrum for EDTA-MXene exhibits some additional peaks that are not seen for MXene. The peaks located at 1708 cm^{-1} and 1045 cm^{-1} are attributed to carboxyl groups and C-N stretching, demonstrating the successful complexing of EDTA on the MXene surface [24]. The peak at 870 cm^{-1} is ascribed to Si-O vibration of EDTA-MXene, which results from the formation of the Si-O bond via the reaction of EDTA-silane alcoholysis and -OH terminals on the MXene surface [24].

Further confirmation of the complexed EDTA-MXene structure is provided by XPS analysis. As shown in Fig. 3c, the XPS survey spectra of MXene and EDTA-MXene revealed the existence of C 1s, O 1s, Ti 2p and F 1s signals in both materials, while the exclusive peaks of Si 2p and N 1s in EDTA-MXene spectrum demonstrate the successful grafting of EDTA. Fig. 3d shows the XPS N 1s core-level spectrum of EDTA-MXene. Deconvoluting the N 1s peak at 399.7 eV yields only one kind of nitrogen-containing functional group as the tertiary amine of EDTA [31].

Deconvolution of the Ti 2p spectra revealed mild oxidation of the as-prepared MXene, with the oxidative product of TiO_2 measured to be 8.4 at%, which was slightly suppressed in the presence of EDTA (TiO_2, 4.3 at %) [32]. The mildly oxidized MXene was also seen from SEM analysis, where the MXene edges are less clearly defined than those of EDTA-MXene, see Table S2 and Figure S8a and S8b of the Supporting Information.

Fig. 4a shows the Cs^+ adsorption isotherms for MXene and EDTA-MXene at 0 V. The data are well-fitted using the Langmuir model and the corresponding fitting parameters are provided in Table S1 of the Supporting Information. The Cs^+ adsorption capacity of MXene was

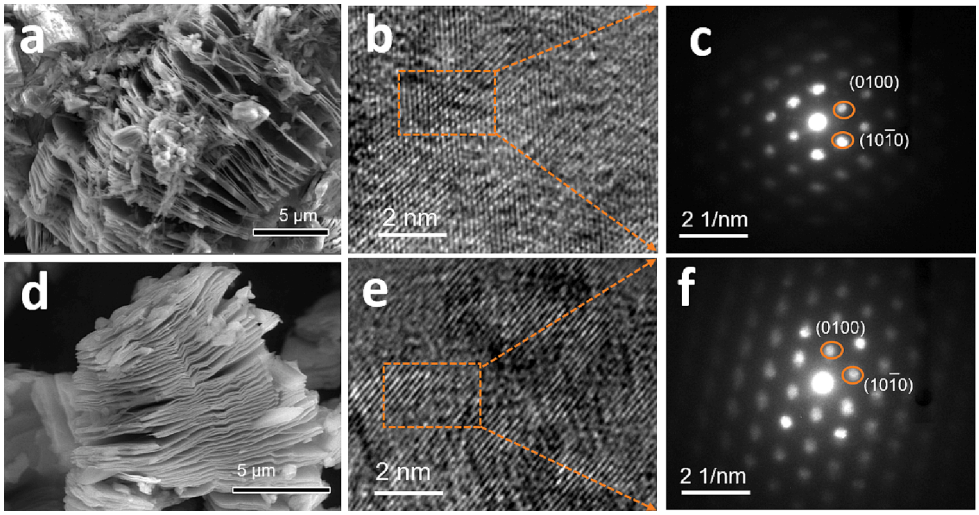

Fig. 2. SEM and TEM images of MXene (a and b) and EDTA-MXene (d and e), with corresponding SAED patterns of MXene (c) and EDTA-MXene (f).

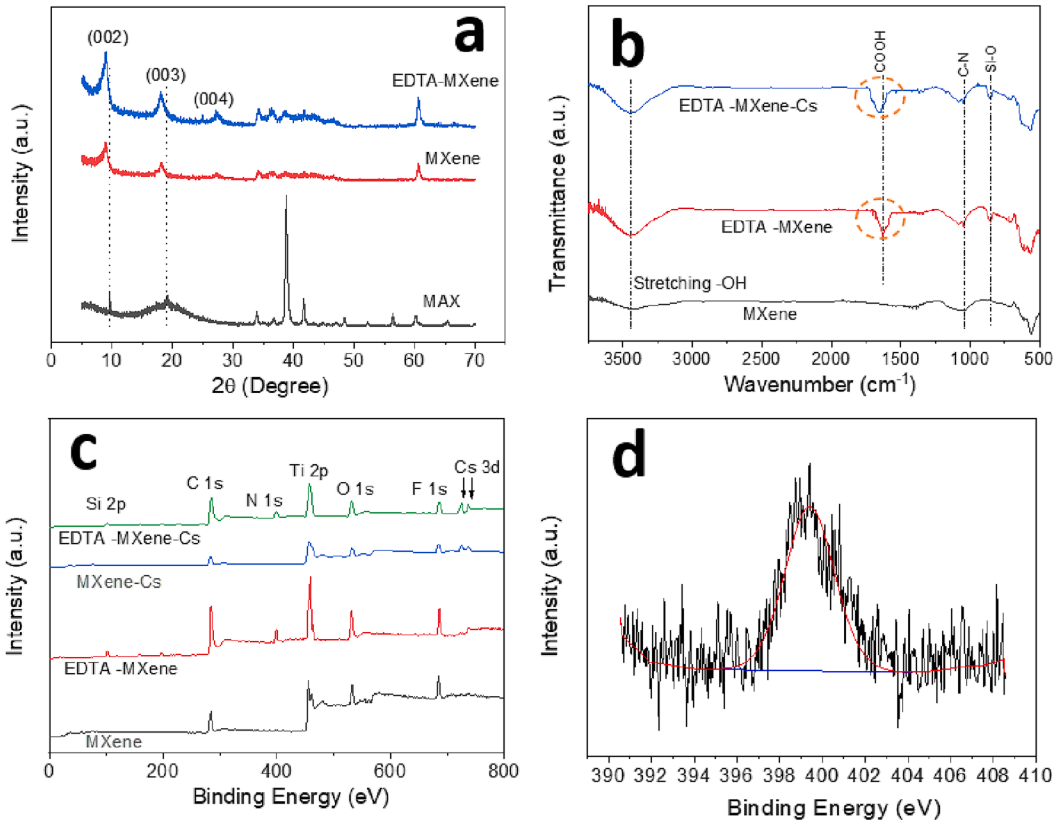

Fig. 3. XRD patterns of MAX, MXene and EDTA-MXene (a); FTIR spectra of MXene and EDTA-MXene and Cs-EDTA-MXene (b); XPS survey spectra of MXene, EDTA-MXene, Cs-MXene and Cs-EDTA-MXene (c); and XPS core-level spectrum of the N 1s peak of EDTA-MXene (d).

0.58 mmol g^{-1} at 0 V, which is enhanced to 1.02 mmol g^{-1} for EDTA-MXene, an improvement of 75% compared to MXene. It is interesting to note a more than doubling in the adsorption capacity (2.07 mmol g^{-1}) of EDTA-MXene when 1.2 V is applied in the CDI cell. The adsorption capacity was found to be comparable to those reported for other materials for example, activated carbon, montmorillonite, graphene oxide, copper hexacyanoferrate and pristine MXene, see Table S3 of the Supporting Information.

The binding of Cs^+ with EDTA-MXene and MXene was evaluated using FTIR and XPS. Fig. 3c shows the XPS survey spectra of Cs-MXene and Cs-EDTA-MXene. The two peaks at 725 and 737 eV are ascribed to Cs $3d_{3/2}$ and Cs $3d_{5/2}$, demonstrating successful adsorption of Cs^+ [14]. Furthermore, the FTIR spectra comparing EDTA-MXene and Cs-EDTA-MXene (Fig. 3b) shows the position of −COOH for Cs-EDTA-MXene to be slightly shifted to a higher wavenumber, 1724 cm^{-1} compared to 1708 cm^{-1} (without Cs^+), which results from the carboxylic transformation to carboxylate, with Cs^+ chemically bound.

Moreover, EDTA is a hexadentate ligand that forms distorted octahedral complexes with metal ions. Cs^+ complexes with EDTA in form of $[CsH_4L]^+$ or $[CsH_2L]^-$, wherein EDTA is abbreviated as H_4L and L represents $C_{10}H_{12}N_2O_8^{4-}$ [33]. Based on this, the proposed interactions between Cs^+ and EDTA are highlighted in Fig. 1, wherein the nitrogen or carbonyl oxygen act as an electron donor for the complexation of Cs^+, forming a stable five-ring structure for its chemical immobilization. Furthermore, the dissociated oxygen of EDTA increases the electronegativity of EDTA-MXene, with the zeta potential being −44 mV compared to −28 mV for MXene. While maybe less significant in retaining the adsorbed ions, the stronger electrostatic attraction can also contribute to enhanced removal of Cs^+ via the electrical double layer effect. These results demonstrate that the enhanced capacity of EDTA-MXene for Cs^+ is indeed from the grafting of carboxyl-rich EDTA-silane on the MXene surface, as intended in our design.

The rate at which target ions can be isolated from process water is a key performance characteristic when considering the suitability of both materials. Fig. 4b compares the adsorption kinetics of MXene and EDTA-MXene in 0.5 mmol L^{-1} Cs^+ solution with 0 and 1.2 V applied in the CDI cell. As shown in Table S1 of the Supporting Information, the R^2 values for all curves were 0.99, confirming that the data is well-fitted by the pseudo-second order rate equation. All curves (Fig. 4b) exhibited a sharp drop in C_t/C_0 within the first 15 min, with Cs^+ removal (loading) efficiencies of 47.6% and 59.8% for MXene at 0 V and 1.2 V, and 73.2% and 97.3 % for EDTA-MXene at 0 V and 1.2 V. The Cs^+ removal efficiency by EDTA-MXene was 99.5% with 1.2 V applied for 120 min, a value much higher than MXene and other common materials such as activated carbon, montmorillonite and graphene oxide, see Table S3 for comparison. The rate constants (k_2) for all experiments were determined by a linear fit and are provided in Figure S4.

To better understand the performance gain of EDTA-MXene compared to MXene, a series of adsorption and desorption studies were undertaken by recirculating 200 mL of 0.5 mmol L^{-1} CsCl solution through the CDI cell, with the applied voltage incrementally increased from 0 to 1.6 V, and for desorption, incrementally lowered from 1.6 V. As shown in Fig. 4c, Cs^+ adsorption by both MXene and EDTA-MXene exhibits three distinct stages: i) between 0 and 0.4 V, the adsorption capacity remains independent of the applied voltage, with ion adsorption mostly physisorption for MXene, and for EDTA-MXene, chemisorption will also contribute leading to a greater adsorption capacity under the same conditions; ii) between 0.4 and 1.2 V, the adsorption capacity increases almost linearly with applied voltage, thus confirming the strong effect of electroadsorption; and iii) beyond 1.2 V the active binding sites become saturated as the maximum adsorption capacity is met.

By lowering the applied voltage to study ion desorption, significant hysteresis is seen for EDTA-MXene but not MXene. No hysteresis

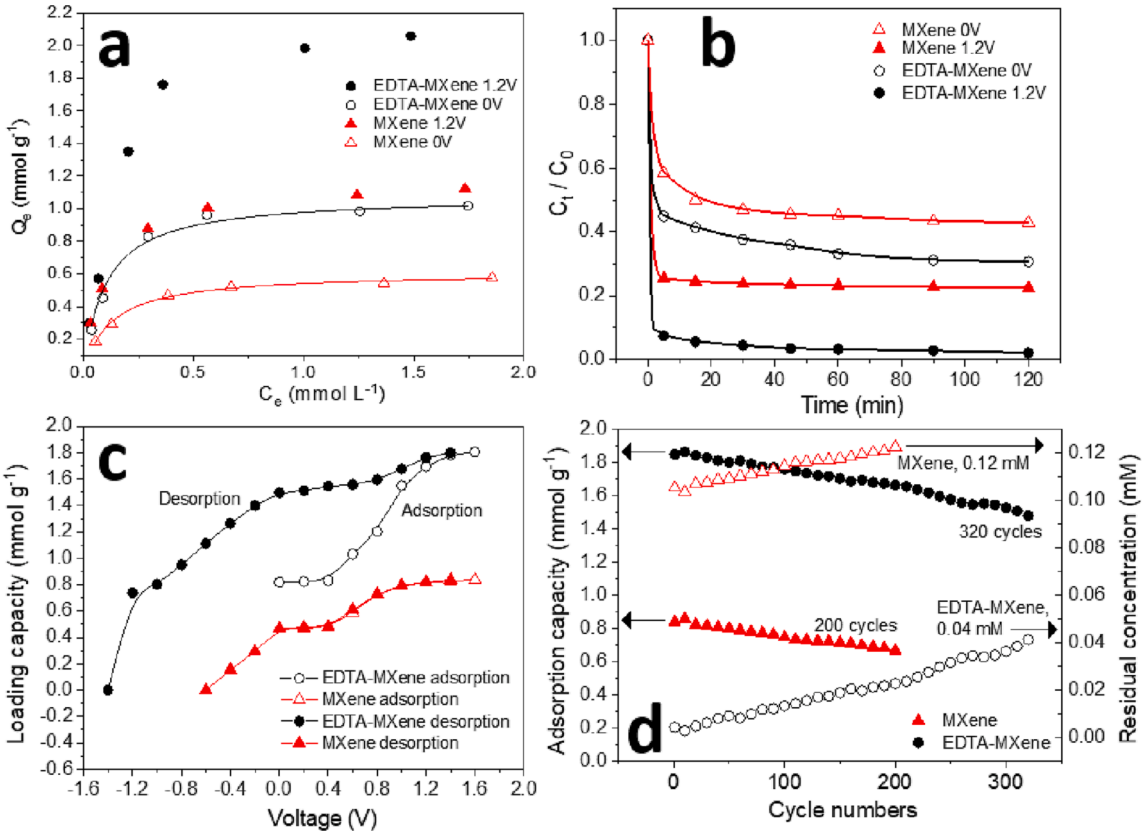

Fig. 4. Adsorption isotherms of MXene and EDTA-MXene at 0 V and 1.2 V (a). The initial concentration of Cs^+ was increased from 0.2 to 2 mmol L^{-1}. The solid lines represent Langmuir isotherm fits; Adsorption kinetics of MXene and EDTA-MXene in 0.5 mmol L^{-1} CsCl solution at 0 V and 1.2 V (b); Step-wise electroadsorption capacity of MXene and EDTA-MXene in CDI (c): open symbols represent the electroadsorption data of increasing applied voltage, while the solid symbols represent the electro-desorption data of decreasing applied voltage after electroadsorption at 1.6 V for 30 min. The initial concentration of the test fluid was 0.5 mmol L^{-1} Cs^+; Cycling performance of MXene and EDTA-MXene when treating 0.5 mmol L^{-1} Cs^+ solutions (d).

confirms that the ion retention energy is comparable during adsorption and desorption, as is the case for Cs-MXene, and is characteristic of the dominant binding mechanism being physisorption via the electrical double layer (EDL) effect. For Cs-EDTA-MXene, the desorption (capacity) curve exceeds the adsorption curve, which suggests that the bound ions are more strongly retained at an equivalent applied voltage, and supports the understanding of a strong chemisorption effect for Cs-EDTA-MXene – see previous discussion on the complexation of EDTA with Cs^+. Cs^+ is retained by EDTA-MXene at 0 V (desorption), with the sorption capacity being 1.5 mmol g^{-1} compared to 0.82 mmol g^{-1} at 0 V (adsorption) initially. This difference verifies the strong chemisorption effect, and to strip the ions to regenerate the sorbent, the applied voltage had to be reversed to −1.4 V, when the sorption capacity was lowered to 0.008 mmol g^{-1}. It is noted that a capacity of 0 mmol g^{-1} means the solution ion concentration after desorption is equal to the initial ion concentration before desorption. Since the CDI cell is operated with an asymmetrical electrode configuration, where the counter electrode has negligible electroadsorption capacity, it is possible to almost fully strip the ions adsorbed to the working electrode and return them to the test fluid. The critical desorption voltage for MXene was found to be smaller due to the absence of any chemisorption. These results demonstrate that EDTA-MXene can effectively immobilize Cs^+, but also by simple reversal of the applied voltage to induce electrostatic repulsion, the chemisorbed ions can be stripped-off without the need to use harsh chemicals to

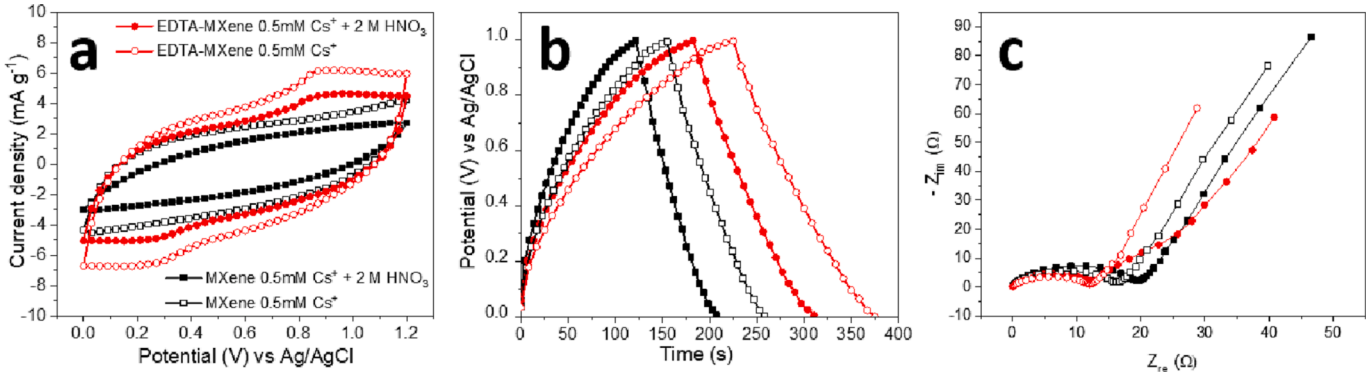

Fig. 5. Cyclic voltammograms at 20 mV s^{-1} (a), galvanostatic charge/discharge at 0.5 A g^{-1} (b), and Nyquist plots of MXene and EDTA-MXene in 0.5 mmol L^{-1} CsCl and 0.5 mmol L^{-1} CsCl with 2 mol L^{-1} HNO_3 (c).

regenerate the adsorbents.

The CV curves of the fabricated electrodes are shown in Fig. 5a. For MXene, both CV curves (without and with HNO_3) are highly rectangular albeit slightly distorted. The distortion results from the charging dynamic which is characteristic of a thick MXene electrode [34]. However, the rectangular shape indicates the pure electrical double-layer capacitive properties of the electrode, and hence, Cs^+ removal is via electroadsorption. By contrast, the CV curves of EDTA-MXene exhibited weak and broad peaks in the region of 0.2 and 0.9 V, suggesting that EDTA-MXene shows pseudo-capacitance with Cs^+, such that the ion binding is not purely electroadsorption, but there is a component of chemisorption. As previously discussed, EDTA-MXene can bind with Cs^+ via the hexadentate ligand of EDTA, wherein the nitrogen or carbonyl oxygen of EDTA acts as an electron donor for Cs^+ complexation, presenting weak and broad peaks in the CV curves. The specific capacitances of EDTA-MXene and MXene in 0.5 mmol L^{-1} CsCl were 245.2 and 154.8 F g^{-1}, confirming the enhanced capacitance of the chemically modified electrode. In 0.5 mmol L^{-1} CsCl and 2 mol L^{-1} HNO_3, the specific capacitances of the two electrodes were lower (EDTA-MXene, 189.4 F g^{-1}; MXene, 112.1 F g^{-1}) due to the presence of H^+, but the test does confirm the retained performance of the electrode in strongly acidic solution, see further discussion below. Such performance is also verified by the GCD profiles (Fig. 5b) which show increased discharge duration of the EDTA-MXene electrode relative to MXene. Fig. 5c shows the Nyquist plots for the EDTA-MXene and MXene electrodes. The width of the semicircle describes the charge-transfer resistance which is measured to be 19 Ω and 12 Ω for MXene and EDTA-MXene (without HNO_3). The smaller interfacial reaction resistance of EDTA-MXene compared to MXene can be attributed to the pseudo-capacitance induced by the chemical modification.

To assess regenerability, MXene and EDTA-MXene were continually cycled between 1.2 V (adsorption) and −1.4 V (desorption) in 0.5 mmol L^{-1} Cs^+ solutions. As shown in Fig. 4d, the performance (loading capacity) of both adsorbents gradually declined after cycling hundreds of times, with the loading capacity of EDTA-MXene decreasing from 1.83 mmol g^{-1} to 1.48 mmol g^{-1} after 320 cycles. However, after cycling hundreds of times, the performance of EDTA-MXene still greatly exceeded that of MXene without cycling, highlighting once again the significant benefit of the chemical modification. The residual Cs^+ concentration increased as the adsorbent performance declined, and for EDTA-MXene, the residual concentration was 0.04 mmol L^{-1} after 320 cycles, much lower than that seen for MXene after only 200 cycles. Those residual concentrations could be further lowered to 10 ppb by a second pass of the feed stream through the CDI cell with the same applied voltage, see Figure S5 (a). Being able to regenerate the adsorbent more than 300 times is a significant step-forward in cycling-performance, yet further work is still needed to overcome this gradual loss in performance.

Fig. S7a shows the gradual drop in capacity retention of MXene and EDTA-MXene to 80% after 200 and 320 cycles, respectively. To understand the mechanism of capacity fade, the fabricated adsorbents were reanalyzed by HR-TEM after long-term cycling. Fig. 6 compares the interlayer structures of the as-synthesized, Cs-adsorbed, and cycled adsorbents (MXene and EDTA-MXene). The interlayer spacings of the as-synthesized MXene (Fig. 6a) and EDTA-MXene (Fig. 6d) were 0.72 and 0.78 nm, respectively. A slight expansion of the MXene interlayer with EDTA is attributed to steric hindrance from the EDTA-silane grafted layer. For Cs-adsorbed, the interlayer spacings of the two adsorbents increased to 0.81 nm for Cs-MXene (Fig. 6b) and 0.92 nm for Cs-EDTA-MXene (Fig. 6e). This interlayer expansion of 10 to 20% is likely due to the increased volume occupied by hydrated Cs ions [35,36]. However, after hundreds of cycles, the interlayer spacings were smaller compared to the as-synthesized and Cs-adsorbed materials. For MXene and EDTA-MXene, the interlayer spacings were 0.58 nm (Fig. 6c) and 0.64 nm (Fig. 6f), respectively. With a smaller interlayer spacing, the number of available binding sites accessible to Cs^+ will be reduced (greater impedance to Cs diffusion through the interlayers), contributing to the observed drop-off in performance. It is hypothesized that the reduced interlayer spacing results from the gradual stripping of functional groups (OH^- and F^-) from the MXene interlayer during repeated Cs adsorption/desorption cycles.

It is also noted that MXenes are propone to oxidative degradation, which may contribute to the capacity fade [37]. SEM inspection of MXene and EDTA-MXene before and after cycling revealed slight differences in the physical appearance of MXene; MXene edges possibly become less clearly defined, but this is not the case for EDTA-MXene, see

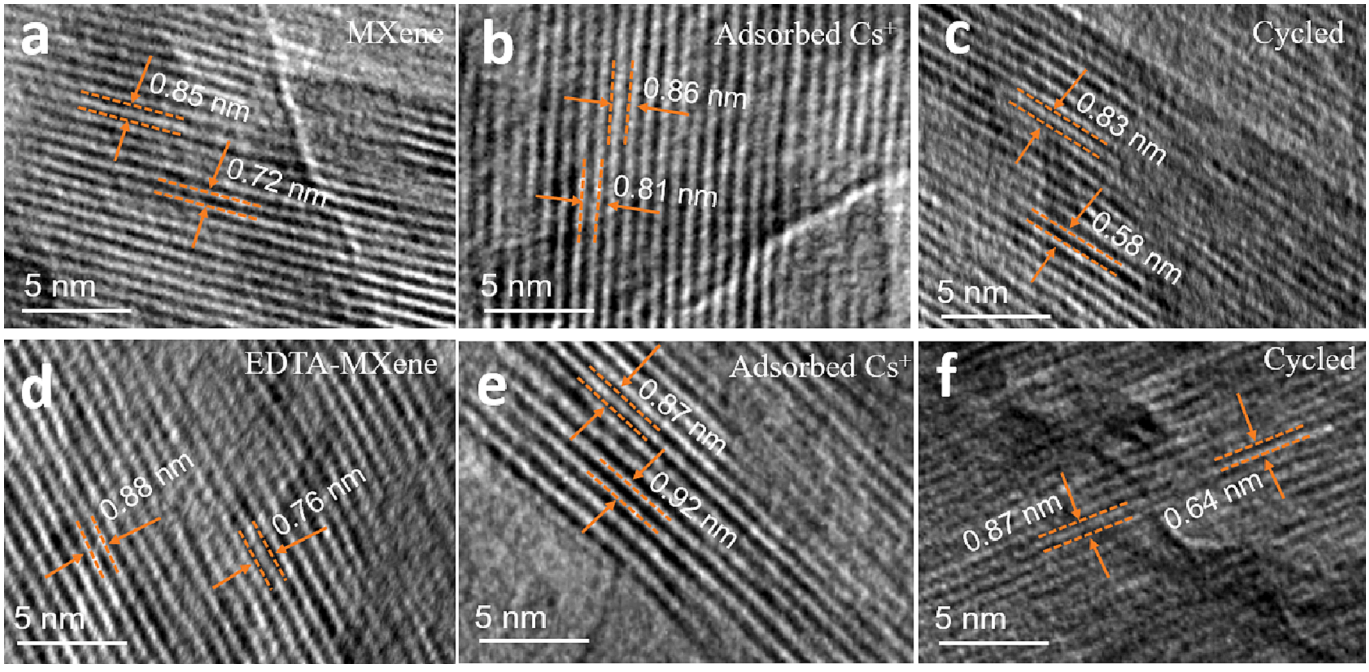

Fig. 6. HR-TEM images of fresh MXene (a); Cs-MXene (b); MXene after 200 cycles without adsorbed Cs (c); fresh EDTA-MXene (d); Cs-EDTA-MXene (e); and EDTA-MXene after 320 cycles without adsorbed Cs (f).

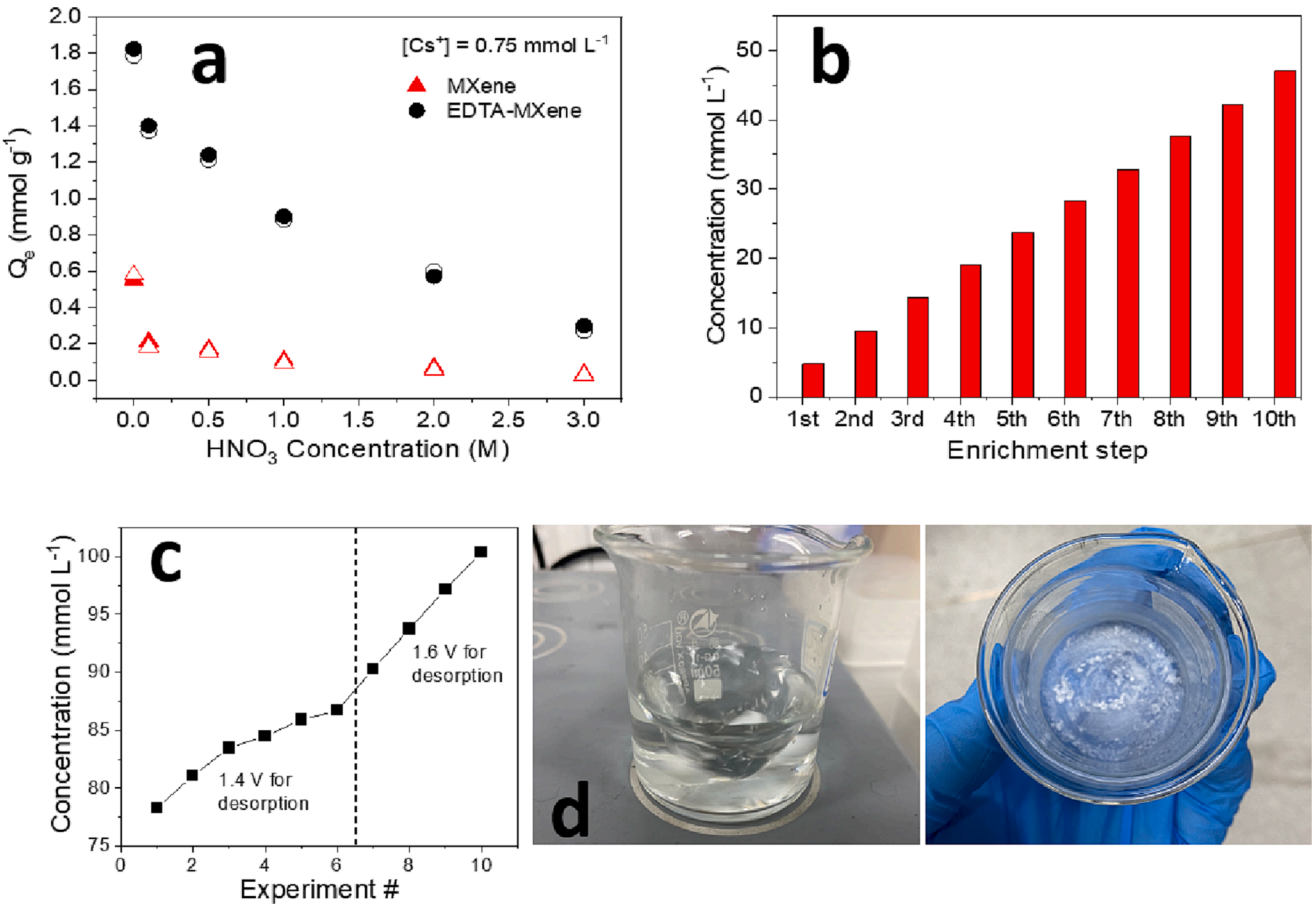

Fig. 7. Competitive adsorption of MXene and EDTA-MXene in 0.75 mmol L^{-1} Cs^+ with HNO_3 concentration varying from 0 to 3 mol L^{-1} (open symbols represent an experimental repeat) (a); Increasing concentrations of Cs in the wastewater following each enrichment step (b); Desorption of Cs into 75 mmol L^{-1} CsCl solution at 1.4 V and 1.6 V (c); Photographs of the concentrated solution after 10 enrichments and the dried solid after solvent evaporation at 40°C for 5 h (d).

Figure S8b and S8d of the Supporting Information. The oxidative product, TiO_2, was detected using XPS, with the TiO_2 content of MXene increasing from 8.4 at% to 13.3 at% after cycling, but remained relatively low at 5.8 at% for EDTA-MXene, see Table S2 of the Supporting Information. This means the grafted EDTA inhibits the oxidative degradation of the electrode and performance loss is more reasonably attributed to interlayer collapse, which should be addressed if the cyclability is to be significantly extended.

Considering the potential use of MXene and EDTA-MXene to remove Cs^+ from process water, it is important to determine any potential detrimental effects of HNO_3 [38,39]. The CDI cell was operated at 1.2 V for 30 min with CsCl solution (0.75 mmol L^{-1}) recirculated with varying concentrations of HNO_3 from 0 to 3 mol L^{-1}. The Cs^+ adsorption capacities of MXene and EDTA-MXene were found to decrease at higher HNO_3 concentrations (Fig. 7a). While the loss in performance can be attributed to increased competitive adsorption of H^+, therefore deactivating available binding sites for Cs^+, it is interesting to note that EDTA-MXene showed reasonable adsorption capacities even up to 2 mol L^{-1} HNO_3, with performance being almost equal to that of MXene in pure water.

Few studies have reported good Cs^+ adsorption in strongly acidic solutions. Jiang et al. [40] tested the performance of an EDTA-functionalized covalent organic framework in pH 1 water, showing performance was 30% of that in weakly acidic solutions. A similar performance loss is seen in the current study. The authors noted better removal of Ag^+, a soft Lewis acid, rather than borderline and hard Lewis acid ions, suggesting a stronger interaction between the soft Lewis acid and soft base of EDTA. A layered metal sulfide ($KlnSnS_4$) has also demonstrated good recovery of Cs^+ in highly acidic solutions, with the authors also attributing its performance to the Hard-Soft-Acid-Base (HSAB) theory, with the soft basic S^{2-} from $[lnSnS_4]_n^{n-}$ layers having a stronger affinity for the soft Lewis acid Cs^+ [41]. For EDTA-MXene, it is likely the HSAB interaction contributes to its sustained performance in strongly acidic solutions, with the complexation interactions become stronger in weakly acidic solutions.

The ability to adsorb Cs^+ was also tested against other relevant competing ions, Sr^{2+} and Ce(IV), with the latter used as a surrogate for U, see Figure S6 of the Supporting Information. For both Ce(IV) and Sr^{2+}, the Cs^+ adsorption capacity decreased with increasing concentration of the competing ion, and in the presence of 2 mol L^{-1} HNO_3, the performance worsened. At the concentrations relevant to the composition of spent fuel dissolver liquor (Ce(IV), 300 g L^{-1}; Sr^{2+}, 1 g L^{-1} and HNO_3), the Cs^+ adsorption capacity was 0.14 mmol g^{-1} with Ce(IV) and 0.25 mmol g^{-1} with Sr^{2+}. However, it is noted that the Cs^+ concentration used is an order of magnitude lower than that found in dissolver liquor (1 g L^{-1}), and so performance should be better. While U could be first separated from the fission products and pose little concern to the extraction method, Sr^{2+} will be present and can mutually compete for binding sites. In dissolver liquor, the concentrations of Cs^+ and Sr^{2+} are almost equivalent, and so when revaluating Fig. S6b, it shows that Cs^+ adsorption remains strong when the concentration of the two competing ions are similar (Cs^+, 0.1 g L^{-1} and Sr^{2+}, 0.2 g L^{-1}).

With very good performance in 2 mol L^{-1} HNO_3, there is potential that such an approach could be adopted in the flowsheets of future fuel recycling, particularly because of its simple application to concentrate the fission product solution for storage. Furthermore, the excellent

stability of the electrode in strong acid demonstrates its suitability to recover cesium from real nuclear effluents. As seen in Figure S10, when soaking the EDTA-MXene electrode in 3 mol L^{-1} HNO_3 for 7 days, the electrode appeared visually unchanged with no apparent structural degradation, thus the composite electrode has potential for long-term and repetitive utilization for cesium recovery from hazardous nuclear effluents.

Enriching a smaller volume of fluid which could be processed to recover useful radioactive elements or be sent for ultimate disposal is advantageous yet is something that is rarely considered in the literature. The current work has studied the ability to consecutively discharge adsorbed ions into an increasingly concentrated wastewater. Fig. 7b shows the build-up of Cs^+ in the wastewater as the adsorbed ions are discharged in 10 enrichment steps. Even as the Cs^+ concentration in the wastewater exceeded 40 mmol L^{-1}, the discharge of adsorbed ions to enrich the wastewater remains unhindered. However, if the adsorbed ions were discharged into a highly concentrated wastewater (c = 75 mmol L^{-1} CsCl, or 10000 ppm), continual enrichment of the wastewater is seen to decline, see Fig. 7c at 1.4 V. To compensate the declining enrichment due to the higher activity coefficient of ions at higher concentrations, increasing the stripping (enrichment) voltage to 1.6 V would overcome the issue (Fig. 7c), although the maximum voltage will be limited by water electrolysis. Fig. 7d shows images of the concentrated wastewater before and after evaporation. The enriched Cs can be crystalized by evaporation to 142 mg of solids (recovered after 10 enrichment steps), with the solids characterized by XRD confirmed to be the CsCl (Fig. S5b), which from a practical perspective could then be smelted to cesium metal via metallothermic reduction [42].

The method demonstrates a feasible strategy to enrich radionuclides while treating radioactive process water by a chemically reactive CDI system. The system is robust to competing ions and avoids the use of secondary chemicals and so does not generate any additional waste streams.

4. Conclusions

A 2D MXene material of EDTA grafted surfaces has been designed and successfully prepared by a facile liquid phase reaction. The composite material is capable of extracting Cs^+ from simulant nuclear process water using CDI. The grafting of EDTA on MXene surface acts as specific adsorption sites to immobilize Cs^+ wherein the nitrogen or carbonyl oxygen act as an electron donor for its complexation, forming a stable five-ring structure. The fabricated electrode exhibits outstanding adsorption capacity of 2.07 mmol g^{-1} at 1.2 V in CDI, and superior recovery of ~ 97.3% at 1.2 V after 15 min. The EDTA-MXene electrode showed excellent durability with the adsorption capacity being retained at more than 80% after 320 cycles. For the first time, good Cs^+ recovery has been shown in strongly acidic solutions (2 mol L^{-1} HNO_3), whereby the HSAB interaction mechanism likely becomes more significant than the complexation interaction. Furthermore, simple reversing of the applied voltage can strip the recovered ions without the need for chemical intervention, hence, enrichment of fission products is readily achieved into small waste packages. The excellent adsorption capacity, kinetics and cycling performance would enable EDTA-MXene to be a highly efficient and robust CDI electrode, showing promise for the practical removal of cesium from hazardous nuclear process water.

CRediT authorship contribution statement

Jiming Lu: Conceptualization, Data curation, Formal analysis, Investigation, Methodology, Writing – original draft, Writing – review & editing. **Qiurong Long:** Data curation, Formal analysis, Investigation. **Yi Liu:** Data curation, Formal analysis, Investigation. **Binda Lu:** Data curation, Formal analysis, Investigation. **Jiaxin Hu:** Data curation, Formal analysis, Investigation. **Fan Yang:** Supervision. **Feng Jiang:** Supervision. **Timothy N. Hunter:** Supervision, Writing – review & editing. **Zhouguang Lu:** Supervision, Writing – review & editing. **David Harbottle:** Conceptualization, Formal analysis, Funding acquisition, Supervision, Writing – review & editing. **Zhenghe Xu:** Conceptualization, Formal analysis, Funding acquisition, Supervision, Writing – review & editing.

Declaration of Competing Interest

The authors declare that they have no known competing financial interests or personal relationships that could have appeared to influence the work reported in this paper.

Data availability

Data will be made available on request.

Acknowledgments

The authors would like to thank financial support from several organizations including Shenzhen Key Laboratory of Interfacial Science and Engineering of Materials (Grant No. ZDSYS20200421111401738); Leading Talents of Guangdong Province Program (Z.X.; 2016LJ06C536); National Natural Science Foundation of China (Grant 51974162); Core Research Facilities, SUSTech, China; Engineering and Physical Sciences Research Council (EPSRC), UK (D.H. and T.N.H.; EP/S032797/1).

Appendix A. Supplementary data

Supplementary data to this article can be found online at https://doi.org/10.1016/j.seppur.2023.123818.

References

[1] A. Baker, A. Fells, M.J. Carrott, C.J. Maher, B.C. Hanson, Process intensification of element extraction using centrifugal contactors in the nuclear fuel cycle, Chem. Soc. Rev. 51 (2022) 3964–3999, https://doi.org/10.1039/d2cs00192f.
[2] M.E. Suss, S. Porada, X. Sun, P.M. Biesheuvel, J. Yoon, V. Presser, Water desalination via capacitive deionization: what is it and what can we expect from it? Energ Environ. Sci. 8 (2015) 2296–2319, https://doi.org/10.1039/c5ee00519a.
[3] C. Zhang, J. Ma, L. Wu, J. Sun, L. Wang, T. Li, T.D. Waite, Flow electrode capacitive deionization (FCDI): recent developments, environmental applications, and future perspectives, Environ. Sci. Technol. 55 (2021) 4243–4267, https://doi.org/10.1021/acs.est.0c06552.
[4] P. Liu, T. Yan, L. Shi, H.S. Park, X. Chen, Z. Zhao, D. Zhang, Graphene-based materials for capacitive deionization, J. Mater. Chem. A 5 (2017) 13907–13943, https://doi.org/10.1039/C7TA02653F.
[5] X. Liu, J. Wang, Electro-assisted adsorption of Cs(I) and Co(II) from aqueous solution by capacitive deionization with activated carbon cloth/graphene oxide composite electrode, Sci. Total Environ. (2020), 141524, https://doi.org/10.1016/j.scitotenv.2020.141524.
[6] X. Liu, J. Wang, Adsorptive removal of Sr^{2+} and Cs^+ from aqueous solution by capacitive deionization, Environ. Sci. Pollut. Res. Int. 28 (2021) 3182–3195, https://doi.org/10.1007/s11356-020-10691-6.
[7] S. Xiang, H. Mao, W. Geng, Y. Xu, H. Zhou, Selective removal of Sr(II) from saliferous radioactive wastewater by capacitive deionization, J. Hazard. Mater. 431 (2022), 128591, https://doi.org/10.1016/j.jhazmat.2022.128591.
[8] S. Yang, G. Wu, J. Song, B. Hu, Preparation of chitosan-based asymmetric electrodes by co-imprinting technology for simultaneous electro-adsorption of multi-radionuclides, Sep. Purif. Technol. 297 (2022), 121568, https://doi.org/10.1016/j.seppur.2022.121568.
[9] L. Kong, M. Su, Z. Mai, H. Li, Z. Diao, Y. Xiong, D. Chen, Removal of uranium from aqueous solution by two-dimensional electrosorption reactor, Environ. Technol. Inno. 8 (2017) 57–63, https://doi.org/10.1016/j.eti.2017.04.001.
[10] J. Zhou, H. Zhou, Y. Zhang, J. Wu, H. Zhang, G. Wang, J. Li, Pseudocapacitive deionization of uranium(VI) with WO_3/C electrode, Chem. Eng. J. 398 (2020), 125460, https://doi.org/10.1016/j.cej.2020.125460.
[11] X. Tang, L. Zhou, J. Xi, J. Ouyang, Z. Liu, Z. Chen, A.A. Adesina, Porous chitosan/biocarbon composite membrane as the electrode material for the electrosorption of uranium from aqueous solution, Sep. Purif. Technol. 274 (2021), 119005, https://doi.org/10.1016/j.seppur.2021.119005.
[12] Y. Zhang, J. Zhou, D. Wang, R. Cao, J. Li, Performance of MXene incorporated MOF-derived carbon electrode on deionization of uranium(VI), Chem. Eng. J. 430 (2022), 132702, https://doi.org/10.1016/j.cej.2021.132702.
[13] A.R. Khan, S.M. Husnain, F. Shahzad, S. Mujtaba-Ul-Hassan, M. Mehmood, J. Ahmad, M.T. Mehran, S. Rahman, Two-dimensional transition metal carbide

($Ti_3C_2T_x$) as an efficient adsorbent to remove cesium (Cs^+), Dalton Trans. 48 (2019) 11803–11812, https://doi.org/10.1039/c9dt01965k.
[14] B.M. Jun, M. Jang, C.M. Park, J. Han, Y. Yoon, Selective adsorption of Cs^+ by MXene ($Ti_3C_2T_x$) from model low-level radioactive wastewater, Nucl. Eng. Technol. 52 (2020) 1201–1207, https://doi.org/10.1016/j.net.2019.11.020.
[15] A. Shahzad, M. Moztahida, K. Tahir, B. Kim, H. Jeon, A.A. Ghani, N. Maile, J. Jang, D.S. Lee, Highly effective prussian blue-coated MXene aerogel spheres for selective removal of cesium ions, J. Nucl. Mater. 539 (2020), 152277, https://doi.org/10.1016/j.jnucmat.2020.152277.
[16] H. Zhang, C.S. Hodges, P.K. Mishra, J.Y. Yoon, T.N. Hunter, J.W. Lee, D. Harbottle, Bio-inspired preparation of clay-hexacyanoferrate composite hydrogels as super adsorbents for Cs^+, ACS Appl. Mater. Interfaces (2020) https://doi.org/10.1021/acsami.0c06598.
[17] Y.K. Kim, S. Kim, Y. Kim, K. Bae, D. Harbottle, J.W. Lee, Facile one-pot synthesis of dual-cation incorporated titanosilicate and its deposition to membrane surfaces for simultaneous removal of Cs^+ and Sr^{2+}, Appl. Surf. Sci. 493 (2019) 165–176, https://doi.org/10.1016/j.apsusc.2019.07.008.
[18] J.Y. Yoon, H. Zhang, Y.K. Kim, D. Harbottle, J.W. Lee, A high-strength polyvinyl alcohol hydrogel membrane crosslinked by sulfosuccinic acid for strontium removal via filtration, J. Environ. Chem. Eng. 7 (2019), 102824, https://doi.org/10.1016/j.jece.2018.102824.
[19] T. Shang, Z. Lin, C. Qi, X. Liu, P. Li, Y. Tao, Z. Wu, D. Li, P. Simon, Q.H. Yang, 3D macroscopic architectures from self-assembled MXene hydrogels, Adv. Funct. Mater. 29 (2019) 1903960, https://doi.org/10.1002/adfm.201903960.
[20] S.K. Hwang, S.M. Kang, M. Rethinasabapathy, C. Roh, Y.S. Huh, MXene: An emerging two-dimensional layered material for removal of radioactive pollutants, Chem. Eng. J. 397 (2020), 125428, https://doi.org/10.1016/j.cej.2020.125428.
[21] C.J. Huang, J.C. Liu, Precipitate flotation of fluoride-containing wastewater from a semiconductor manufacturer, Water Res. 33 (1999) 3403–3412, https://doi.org/10.1016/S0043-1354(99)00065-2.
[22] W. Sun, S.A. Shah, Y. Chen, Z. Tan, H. Gao, T. Habib, M. Radovic, M.J. Green, Electrochemical etching of Ti_2AlC to Ti_2CT_x (MXene) in low-concentration hydrochloric acid solution, J. Mater. Chem. A 5 (2017) 21663–21668, https://doi.org/10.1039/c7ta05574a.
[23] C.E. Shuck, A. Sarycheva, M. Anayee, A. Levitt, Y. Zhu, S. Uzun, V. Balitskiy, V. Zahorodna, O. Gogotsi, Y. Gogotsi, Scalable Synthesis of $Ti_3C_2T_x$ MXene, Adv. Eng. Mater. 22 (2020) 1901241, https://doi.org/10.1002/adem.201901241.
[24] P. Liu, T. Yan, J. Zhang, L. Shi, D. Zhang, Separation and recovery of heavy metal ions and salt ions from wastewater by 3D graphene-based asymmetric electrodes via capacitive deionization, J. Mater. Chem. A 5 (2017) 14748–14757, https://doi.org/10.1039/c7ta03515b.
[25] J. Lu, P. Kumar Mishra, T.N. Hunter, F. Yang, Z. Lu, D. Harbottle, Z. Xu, Functionalization of mesoporous carbons derived from pomelo peel as capacitive electrodes for preferential removal/recovery of copper and lead from contaminated water, Chem. Eng. J. 433 (2022), 134508, https://doi.org/10.1016/j.cej.2022.134508.
[26] H. Zhang, Y.K. Kim, T.N. Hunter, A.P. Brown, J.W. Lee, D. Harbottle, Organically modified clay with potassium copper hexacyanoferrate for enhanced Cs^+ adsorption capacity and selective recovery by flotation, J. Mater. Chem. A 5 (2017) 15130–15143, https://doi.org/10.1039/c7ta03873a.
[27] J. Li, X. Wang, H. Wang, S. Wang, T. Hayat, A. Alsaedi, X. Wang, Functionalization of biomass carbonaceous aerogels and their application as electrode materials for electro-enhanced recovery of metal ions, Environ. Sci, Nano 4 (2017) 1114–1123, https://doi.org/10.1039/c7en00019g.
[28] Y.H. Kim, K. Tang, J. Chang, K. Sharma, S. Yiacoumi, R.T. Mayes, H.Z. Bilheux, L. J. Santodonato, C. Tsouris, Potential limits of capacitive deionization and membrane capacitive deionization for water electrolysis, Sep. Sci. Technol. 54 (2019) 2112–2125, https://doi.org/10.1080/01496395.2019.1608243.
[29] M. Naguib, M. Kurtoglu, V. Presser, J. Lu, J. Niu, M. Heon, L. Hultman, Y. Gogotsi, M.W. Barsoum, Two-dimensional nanocrystals produced by exfoliation of Ti_3AlC_2, Adv. Mater. 23 (2011) 4248–4253, https://doi.org/10.1002/adma.201102306.
[30] Q. Peng, J. Guo, Q. Zhang, J. Xiang, B. Liu, A. Zhou, R. Liu, Y. Tian, Unique lead adsorption behavior of activated hydroxyl group in two-dimensional titanium carbide, J. Am. Chem. Soc. 136 (2014) 4113–4116, https://doi.org/10.1021/ja500506k.
[31] R.J.J. Jansen, H. van Bekkum, XPS of nitrogen-containing functional groups on activated carbon, Carbon 33 (1995) 1021–1027, https://doi.org/10.1016/0008-6223(95)00030-H.
[32] C. Peng, X. Yang, Y. Li, H. Yu, H. Wang, F. Peng, Hybrids of two-dimensional Ti_3C_2 and TiO_2 exposing 001 facets toward enhanced photocatalytic activity, ACS Appl. Mater. Interfaces 8 (2016) 6051–6060, https://doi.org/10.1021/acsami.5b11973.
[33] S. Beck, Fragmentation behavior of EDTA complexes under different activation conditions, J. Mass Spectrom. 56 (2021), e4775, https://doi.org/10.1002/jms.4775.
[34] P. Srimuk, F. Kaasik, B. Krüner, A. Tolosa, S. Fleischmann, N. Jäckel, M.C. Tekeli, M. Aslan, M.E. Suss, V. Presser, MXene as a novel intercalation-type pseudocapacitive cathode and anode for capacitive deionization, J. Mater. Chem. A 4 (2016) 18265–18271, https://doi.org/10.1039/c6ta07833h.
[35] J. Halim, M.R. Lukatskaya, K.M. Cook, J. Lu, C.R. Smith, L.A. Naslund, S.J. May, L. Hultman, Y. Gogotsi, P. Eklund, M.W. Barsoum, Transparent Conductive Two-Dimensional Titanium Carbide Epitaxial Thin Films, Chem. Mater. 26 (2014) 2374–2381, https://doi.org/10.1021/cm500641a.
[36] J. Li, X. Yuan, C. Lin, Y. Yang, L. Xu, X. Du, J. Xie, J. Lin, J. Sun, Achieving high pseudocapacitance of 2D titanium carbide (MXene) by cation intercalation and surface modification, Adv. Energ. Mater. 7 (2017) 1602725, https://doi.org/10.1002/aenm.201602725.
[37] F. Cao, Y. Zhang, H. Wang, K. Khan, A.K. Tareen, W. Qian, H. Zhang, H. Agren, Recent advances in oxidation stable chemistry of 2D MXenes, Adv. Mater. 34 (2022), e2107554, https://doi.org/10.1002/adma.202107554.
[38] W. Mu, S. Du, X. Li, Q. Yu, H. Wei, Y. Yang, S. Peng, Removal of radioactive palladium based on novel 2D titanium carbides, Chem. Eng. J. 358 (2019) 283–290, https://doi.org/10.1016/j.cej.2018.10.010.
[39] M.W. Davis, C.B. Bowers, Extraction of cesium and strontium from nuclear waste, in, EP (1988).
[40] Y. Jiang, C. Liu, A. Huang, EDTA-Functionalized Covalent Organic Framework for the Removal of Heavy-Metal Ions, ACS Appl. Mater. Interfaces 11 (2019) 32186–32191, https://doi.org/10.1021/acsami.9b11850.
[41] J.H. Tang, J.C. Jin, W.A. Li, X. Zeng, W. Ma, J.L. Li, T.T. Lv, Y.C. Peng, M.L. Feng, X.Y. Huang, Highly selective cesium(I) capture under acidic conditions by a layered sulfide, Nat. Commun. 13 (2022) 658, https://doi.org/10.1038/s41467-022-28217-8.
[42] E.J. Skach Jr, K.G. Claus, M.R. Earlam, Metallothermic reduction or rare earth metals, in, Google Patents (1991).